Available online at www.sciencedirect.com
SCIENCE DIRECT®
ELSEVIER
Earth and Planetary Science Letters 217 (2003) 85–95
EPSL
www.elsevier.com/locate/epsl

Linear elastic fracture mechanics explains the past and present evolution of the Aegean

Rolando Armijo *, Frédéric Flerit, Geoffrey King, Bertrand Meyer

Laboratoire de Tectonique, IPGP, 4, place Jussieu, 75252 Paris Cedex 5, France

Received 19 May 2003; received in revised form 15 October 2003; accepted 15 October 2003

Abstract

Geologically the deformation in the Anatolian–Aegean region has been dominated by two processes: the propagation of the North Anatolian fault associated with the extrusion of the Anatolian plateau, and the north–south stretching of the Aegean. We model GPS data in the context of this understanding. Localised deformation zones are represented by dislocation elements which extend from the base of the lithosphere to the locking depth at the base of the seismogenic layer. Unlike other GPS interpretations our models incorporate geological and seismological constraints to provide a robust description of the present-day deformation of the Anatolian–Aegean region. We then show that the present-day deformation observed by GPS today is consistent with the continuation of the geological processes that started in the Tertiary. Our approach is also consistent with the lithosphere preserving long-term elastic strength and with the concepts of linear elastic fracture mechanics applying at a large scale.

Keywords: Aegean; North Anatolian Fault; GPS modelling; elasto-plastic lithosphere; fracture mechanics; tectonics

1. Introduction

The knowledge of the geological evolution of the Aegean is crucial to the approach we present here. Extension in the Aegean started between 20 and 15 Ma [1–4] and has been mostly confined to a small number of major structures that extend through the lithosphere (Fig. 1a) [5]. The North Anatolian Fault (NAF) was born in eastern Turkey between 10 and 13 Ma [6,7] and extended by propagation to the west (Fig. 1b). The fault reached the site of the present Marmara Sea at 5 Ma [5,8,9] before entering and modifying the active extension in the Aegean [5]. As the fault propagated into the Aegean it suppressed activity on its compressional side and increased it on the extensional side (Fig. 1b). Features such as the North Aegean Trough and the Evvia fault system increased in extension rate and finally, at 1 Ma, the Corinth Rift increased in activity from about 1 mm/yr to about 10 mm/yr [5]. The NAF does not yet directly connect to the Corinth Rift suggesting that the increase of activity results from more distributed deformation ahead of the advancing NAF [5].

Two types of mechanical model have been proposed to explain the geological evolution of the

* Corresponding author. Tel.: +33-1-4427-2497; Fax: +33-1-4427-2440.
E-mail address: armijo@ipgp.jussieu.fr (R. Armijo).

0012-821X/03/$ – see front matter © 2003 Elsevier B.V. All rights reserved.
doi:10.1016/S0012-821X(03)00590-9

Aegean. The earliest supposed that the Aegean had stretched and subsided by a viscous process to give thin crust and upper mantle and a high heat flow in the centre of the basin [10–13]. The role of the NAF and its relation to Aegean extension was scarcely addressed in these models and viscous models also fail to address the geological evidence suggesting localisation of deformation. A modification of continuum models incorporated rigid blocks floating in the viscous lithosphere, which drives the motion, much like 'blocks of ice floating in a river' [14–17]. While these models require widespread decoupling of the brittle seismogenic zone from the underlying viscous lithosphere, the inferred continuous velocity field could be tested with the new space geodesy data. Yet, the velocity field derived from the GPS measurements for the Anatolia–Aegean region strongly suggests localisation of deformation consistent with the geological evidence [18–20]. As a response, rigid lithospheric block models have been proposed as an extreme alternative to continuum deformation, but again fail to be consistent with geological observations [20,21].

Here we offer a third view based on concepts of fracture mechanics, which allows us to incorpo-

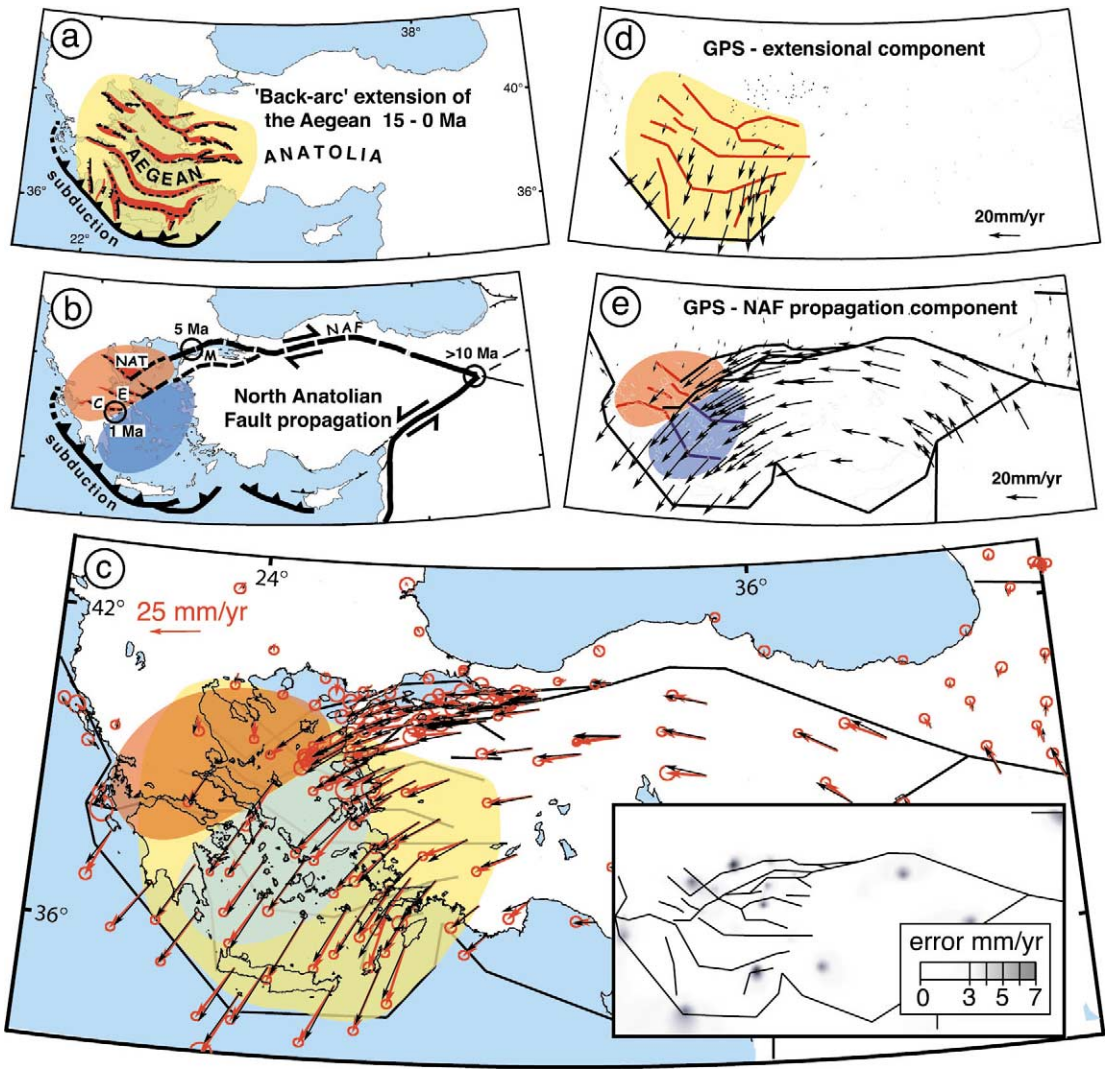

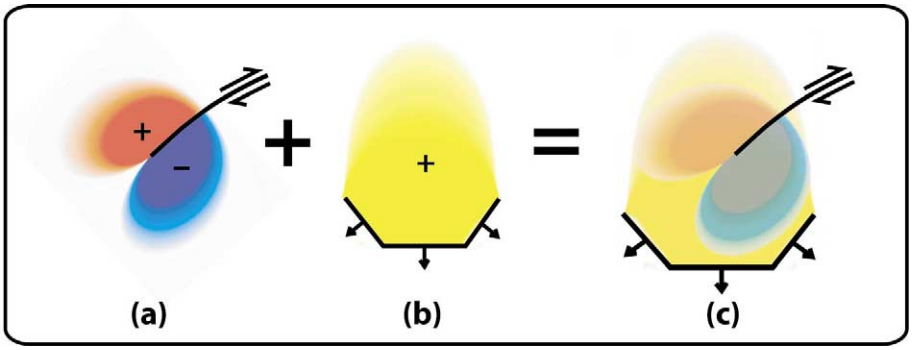

Fig. 2. (a) Areal strain associated with a shear crack terminating with an elliptical slip distribution. Red indicates extension and blue contraction. (b) Areal strain resulting from pull along arc. Yellow indicates areal extension. (c) Superposition of the areal strain due to the terminating crack and the arc pull.

rate both the geodetic and the geological constraints, in keeping with the idea that the present is a key to the past and vice versa.

2. The mechanical model

In our alternative view to continuum and block models, almost all deformation is concentrated along block boundaries, but some internal deformation is possible as suggested earlier (e.g. [22,23]). The mechanical relation between the localised deformation and distributed deformation is most readily understood when it is appreciated that faults evolve by propagation [24,25] and by applying the concepts of fracture mechanics. Thus our models account for elastic strains and damage zones in the intervening regions between block boundaries. As major faults cut and propagate in the continental lithosphere, damage zones are created. Although similar to those observed in engineering materials those in the Earth are larger than the restricted regions found around the crack tips of materials adopted by engineers [26,27].

In this view, the early stretching of the Aegean is considered to result from motion of the sub-

←

Fig. 1. (a) The system of major structures that have been responsible for Aegean extension over the last 15 Myr. It appears that most of the extension was accommodated by four or possibly five such features. The origin of the extension is often attributed to 'back-arc' extension due to 'slab-pull' from the Aegean subduction. The main extensional structures are shaded in red and the overall zone where geological extension is observed is shaded in light yellow. (b) The evolution of the NAF. Circles indicate approximately where the first effects of the fault can be dated and the dates of arrival of the propagating fault are shown. The fault has not yet cut through to join with the subduction boundary and as a result creates a large zone of deformation (damage zone). The region where this zone is extensional is shaded light red and where it is contractional blue. The main extensional structures (shaded in plain red) are the North Aegean Trough (NAT), the Evvia fault system (E) and the Corinth Gulf (C). M denotes Marmara Sea. (c) The elements (black lines) used to model (black arrows) the GPS velocity vectors (red arrows). The 95% confidence ellipses (red) are shown. With few exceptions any misfit between the observed and modelled velocities falls within the errors. The red (superposed on yellow) shading indicates where the elements are required to have rapid opening to model the observations and the blue (superposed on yellow) where the rate of opening is modest. Details of the location and displacement direction and rate for the elements of the models are provided in the Supplementary material. (d) The structures associated with the long-term extension in the Aegean (yellow) are shown in red. These are given opening rates consistent with long-term geological rates. The Aegean subduction is given a rate that absorbs the extension. The black vectors are plotted at the same points as the GPS measurements and represent the part of the velocity field that can be attributed to Aegean extension alone. (e) The elements used to model the NAF propagation without the component due to Aegean extension are shown in black, blue and red. The vectors for central and eastern Turkey are consistent with the rates predicted by the Anatolia–Eurasia rotation. Red elements in the red shaded zone are associated with extension and blue elements in the blue shaded zone with contraction. Subduction is adjusted along the Hellenic subduction to absorb the extrusion associated with motion of the NAF. The red elements from north to south correspond to the North Aegean Trough, the Evvia fault system and the Gulf of Corinth.

duction system away from Europe resulting in lithospheric structures that extended by propagation east and west into Anatolia and mainland Greece. Stretching was distributed between four or five zones rather than concentrating on one [5]. This can be explained by a simple gravitational modification of fracture processes [24]. Topography associated with extension does work against gravity. Thus, unlike a crack in the laboratory, which becomes progressively easier to open, the deeper a rift valley becomes the greater are the forces required to open it further.

Fracture mechanics models are commonly based on elastic solutions although it is understood that some regions cannot behave elastically [24,27]. The basic principles required to understand the NAF–Aegean system are shown in Fig. 2. Fig. 2a shows strain at the end of a shear crack with red and blue indicating areal extension and contraction. Fig. 2b shows the strain that results from pull along a simplified arc with yellow indicating areal extension. These different colours are also used in Fig. 1 to distinguish areas influenced by strains due to the NAF and the Aegean arc respectively. Although such models yield insight into the general nature of the damage zone of the NAF, features like the Evvia and Corinth rifts and features in the south central Aegean are not specifically included.

Sufficient data are now available, not only to test propagation models against contemporary motions, but also to include features such as the Corinth Rift in models of the GPS velocity field allowing us to create a more complete mechanical model for the relation between the NAF and the Aegean.

3. Modelling present-day motion using GPS data

Geological models of the categories discussed above and proposed for various parts of the world are now subject to tests using GPS data [23,28–32]. In general, as the density of GPS coverage has improved, continuum models have been found to be inadequate and have given way to models in which deformation is mostly localised on a small number of structures that extend to the base of the lithosphere [23,33–36]. Modelling of GPS data in Greece and Turkey [19,20] is no exception. The vectors have been modelled using undeforming lithospheric blocks separated by continuously creeping faults that extend from the 'locking depth' at the bottom of the seismogenic zone to the base of the lithosphere. In these models the blocks are undeforming like the rigid blocks of plate tectonics except for elastic strains associated with earthquakes in a thin seismogenic zone. The criterion for a 'good fit' is that internal block deformation is minimised. However, although the Anatolian–Aegean GPS vectors can be modelled using blocks [20], the displacement conditions found at the block boundaries are incompatible with geological evidence. For example, block modelling of the Sea of Marmara region very clearly encounters such incompatibilities [21,37]. An alternative strategy shown by Flerit et al. [38] is to represent the major features by dislocations in the same way as for block models, but require that the direction of motion along the boundaries is consistent with geological constraints. The dislocations are not required to divide the region into blocks, but can terminate where geological evidence suggests that motion on deeper structures tapers out. These 'blocks' can deform, a view that is consistent with some deformation (both elastic and plastic) being associated with the continuing geological evolution of the system by propagation processes [24].

4. Modelling present-day motion of the NAF and in the Aegean

The main geologically active structures of the Anatolian–Aegean region are shown in Fig. 1a,b. Fig. 1a shows the structures associated with the long-term geological extension of the Aegean and Fig. 1b shows the structures associated with NAF propagation. Fig. 1c shows the elements used for modelling derived from these structures together with the observed and modelled GPS vectors. The modelling technique using dislocation elements is conventional and described in the Appendix where the location and displacement conditions used to create the model in Fig. 1c are tabulated.

The slip vectors that fit the GPS velocity field are found by forward modelling. The motions on certain boundaries are known and are not free parameters in the modelling (the vectors are fixed in both amplitude and direction). These include relative plate motions (Arabia, Africa, Anatolia and Eurasia) [20, 39]. For the other boundaries, geological and seismological information is used to constrain the vector directions, with the amplitudes being determined to fit the observed velocity vectors. The procedure for arriving at a final model for the velocity field is by trial and error in the same way as that described by Flerit et al. [38]. Provided that the element geometry selected from the geology is correct the solution is unique within the limits of data error. The geological and seismological data included in our models provide major constraints not adopted in other approaches. The errors in the fit are shown in the inset of Fig. 1c, where the modulus of the difference between the observed and modelled vectors is shaded. With few exceptions (grey blobs in the inset) the fit is within the quoted error ellipses [20]. The remaining misfits are not systematically distributed indicating that individual sites are anomalous or are affected by small local structures [38].

For northern Turkey the displacement changes abruptly as the NAF is crossed indicating the same deformation localisation that is observed geologically [7]. In the Aegean, slip amplitudes change less abruptly and vary progressively at the latitude of the Peloponnesus. The observed deformation thus seems similar to that observed geologically and consequently it seems cogent to ask if the GPS velocity vectors, like the geological deformation, can be decomposed into Aegean extension and the effects of NAF propagation.

5. Decomposing the present-day deformation field

Fig. 1d shows elements that represent faults that are known to have pre-dated the arrival of the NAF. The motion on these elements is chosen to be consistent with rates for long-term Aegean extension. Fig. 1e shows motion due to the NAF and those parts of the pre-existing Aegean elements that would be re-activated by the NAF motion. The elements in the red region experience extension and those in the blue region contraction. In the absence of Aegean extension, elements in the blue region would represent reverse faulting. The effect of the superposition (Fig. 2c) of the two fields (Fig. 1a,b) is to suppress deformation in the blue region leaving no significant contraction and reverse faulting in the Aegean.

The decomposition of the velocity field is arbitrary in a mathematical sense. The decomposition is useful if it is consistent with the two processes summarised in Fig. 1 and identified by the geological history. One field must be consistent with accommodating the strain field associated with the termination of the NAF and the second with the extension resulting from the subduction processes alone. The slip determined on the elements for each separated velocity field (Fig. 1d,e) satisfies these conditions.

6. Conclusions

Geological studies show that the Aegean–NAF system can be understood as the result of two superposed systems: the propagating NAF that results from the westward motion of Anatolia due to extrusion and the extension of the Aegean related to subduction processes. The structures that have been involved in the geological evolution are readily identified. The direction of motion on these features can be determined and, for many of them, the rates of motion are also known.

Such information has not been used in previous models to constrain present-day motion, which have proved to be inconsistent with simple geological observations. When geological and seismological information is used to constrain parameters the predicted GPS velocity vectors fit the data to within the errors of observation.

The model can be split into two parts, one due to on-going Aegean extension and one to on-going NAF propagation. The ability to do this provides substantial support for geological models that consider that the Anatolian–Aegean lithosphere retains long-term strength and that major

Table A1
Slip rates on elements

Element number	Element start		Element end		locking depth	Components	
	Long	Lat	Long	Lat	(km)	(mm/yr)	
						Right Lateral	Opening
1	41.68	42.35	53.15	38.07	12	0	−8
2	53.15	38.07	63.21	32.79	12	0	−8
3	41.09	39.15	39.74	39.6	12	24	−6
4	39.74	39.6	35.38	41.09	12	24	0
5	35.38	41.09	33.99	41.16	12	24	−3
6	33.99	41.16	32.54	40.85	12	22	−8
7	32.54	40.85	30.89	40.57	12	12	0
8	30.89	40.57	30.03	40.43	12	5	1
9	30.03	40.43	29.65	40.22	12	5	0
10	29.65	40.22	29.24	40.19	12	5	3
11	29.24	40.19	27.7	40.15	12	4	3
12	27.7	40.15	26.82	39.5	12	2	−1
13	26.82	39.5	25.54	39.38	12	2	4
14	25.54	39.38	25.28	39.21	12	5	0
15	25.28	39.21	24.64	38.93	12	12	2
16	24.64	38.93	24.39	38.7	12	12	−2
17	24.39	38.7	23.92	38.26	12	7	−1
18	23.22	38.05	22.87	38.13	12	−3	13
19	22.87	38.13	22.53	38.2	12	−2	11
20	22.53	38.2	22.18	38.28	12	−1	9
21	22.18	38.28	21.84	38.35	12	−1	7
22	21.84	38.35	21.51	38.25	12	3	4
23	21.51	38.25	21.18	38.15	12	2	3
24	21.18	38.15	20.85	38.05	12	1	1
25	20.85	38.05	20.15	38.12	12	0	0
26	20.15	38.12	20.47	37.39	4	19	−14
27	20.47	37.39	21.37	36.68	4	14	−41
28	21.37	36.68	22.25	35.97	4	14	−42
29	22.25	35.97	23.11	35.25	4	14	−43
30	23.11	35.25	23.96	34.53	4	14	−44
31	23.96	34.53	24.83	34.55	4	−24	−44
32	24.83	34.55	25.7	34.58	4	−21	−43
33	25.7	34.58	26.58	34.59	4	−17	−43
34	26.58	34.59	27.45	34.6	4	−13	−42
35	27.45	34.6	27.79	34.93	4	−37	−22
36	27.79	34.93	28.14	35.25	4	−32	−22
37	28.14	35.25	28.49	35.58	4	−28	−21
38	28.49	35.58	28.53	35.85	4	−31	−6
39	28.53	35.85	28.58	36.12	4	−30	−3
40	28.58	36.12	28.62	36.39	4	−29	−1
41	28.62	36.39	29.14	35.96	12	4	−20
42	29.14	35.96	29.65	35.52	12	4	−19
43	29.65	35.52	30.49	35.27	12	−5	−17
44	30.49	35.27	31.33	35.01	12	−5	−16
45	31.33	35.01	32.17	34.75	12	−5	−14
46	32.17	34.75	32.99	34.48	12	−5	−12
47	32.99	34.48	34.34	35.15	12	−12	−2
48	34.34	35.15	35.71	35.81	12	−12	1
49	35.71	35.81	36.29	37.11	12	−8	11
50	36.29	37.11	41.09	39.15	12	−10	2

Table A1 (*Continued*).

Element number	Element start		Element end		locking depth	Components (mm/yr)	
	Long	Lat	Long	Lat	(km)	Right Lateral	Opening
51	30.89	40.57	30.25	40.72	12	6	3
52	30.03	40.43	28.1	40.46	12	4	1
53	28.1	40.46	25.54	39.38	12	2	0
54	32.54	40.85	31.94	40.82	12	12	0
55	31.94	40.82	30.25	40.72	12	12	0
56	30.25	40.72	29.28	40.73	12	18	1
57	29.28	40.73	28.86	40.9	4	17	8
58	28.86	40.9	27.45	40.8	4	19	0
59	27.45	40.8	26.61	40.53	12	20	1
60	26.61	40.53	25.29	40.21	12	20	5
61	25.29	40.21	23.81	39.23	12	20	−1
62	23.81	39.23	23.51	39.41	12	0	11
63	23.51	39.41	23.2	39.58	12	0	9
64	23.2	39.58	22.89	39.76	12	0	6
65	22.89	39.76	22.57	39.93	12	0	4
66	29.99	39.82	29.21	40.19	12	0	0
67	29.93	39.47	28.71	39.47	12	0	4
68	27.45	39.6	26.82	39.5	12	0	3
69	28.83	38.18	28.43	38.28	12	−1	4
70	28.43	38.28	28.04	38.38	12	−2	4
71	28.04	38.38	27.65	38.47	12	−2	5
72	27.65	38.47	26.69	38.44	12	0	6
73	26.69	38.44	26.45	38.86	12	−6	2
74	29.52	39.06	29.02	39.17	12	−1	4
75	29.02	39.17	28.52	39.27	12	−1	4
76	28.52	39.27	28.02	39.38	12	−2	5
77	28.02	39.38	26.88	39.12	12	1	5
78	26.88	39.12	26.45	38.86	12	2	3
79	26.45	38.86	25.28	39.21	12	0	6
80	25.28	39.21	24.65	39.58	12	0	5
81	24.65	39.58	24.02	39.95	12	0	3
82	24.02	39.95	23.38	40.31	12	0	2
83	23.92	38.26	23.06	38.2	12	0	3
84	23.57	38.56	23.17	38.73	12	0	6
85	23.17	38.73	22.25	38.9	12	0	4
86	30.1	37.91	29.82	37.9	12	0	3
87	29.82	37.9	29.54	37.9	12	0	4
88	29.54	37.9	29.25	37.89	12	0	6
89	29.25	37.89	28.97	37.89	12	0	8
90	28.97	37.89	27.2	37.83	12	0	8
91	27.2	37.83	26.81	37.83	12	0	8
92	26.81	37.83	26.42	37.82	12	0	5
93	26.42	37.82	26.03	37.8	12	0	3
94	26.03	37.8	25.64	37.79	12	0	2
95	25.64	37.79	25.2	38	12	0	0
96	25.2	38	24.76	38.2	12	0	0
97	24.76	38.2	24.31	38.4	12	0	0
98	24.39	38.7	23.82	38.85	12	0	8
99	23.82	38.85	23.37	39.12	12	0	5
100	28.96	37.26	28.62	37.2	12	0	2
101	28.62	37.2	28.29	37.14	12	0	4

Table A1 (*Continued*).

Element number	Element start		Element end		locking depth	Components (mm/yr)	
	Long	Lat	Long	Lat	(km)	Right Lateral	Opening
102	28.29	37.14	27.57	36.9	12	0	5
103	27.57	36.9	26.86	36.66	12	0	5
104	26.86	36.66	26.15	36.41	12	0	5
105	26.15	36.41	25.61	36.44	12	0	3
106	25.61	36.44	25.07	36.46	12	0	2
107	25.07	36.46	24.53	36.49	12	0	1
108	24.53	36.49	24.1	37.01	12	0	0
109	24.1	37.01	23.66	37.53	12	0	0
110	23.66	37.53	23.22	38.05	12	0	0
111	28.18	36.57	27.8	36.49	12	0	0
112	27.8	36.49	27.43	36.42	12	0	0
113	27.43	36.42	27.05	36.34	12	0	0
114	27.05	36.34	26.97	36.05	12	0	3
115	26.97	36.05	26.89	35.76	12	0	4
116	26.89	35.76	26.81	35.47	12	0	4
117	22.77	37.53	22.94	37.19	12	0	0
118	22.94	37.19	23.12	36.85	12	0	1
119	23.12	36.85	23.29	36.51	12	0	1
120	23.29	36.51	23.38	36.09	12	0	2
121	23.38	36.09	23.47	35.67	12	0	2
122	23.47	35.67	23.56	35.26	12	0	2
123	16.94	43.06	20.61	38.92	12	8	−2
124	20.61	38.92	20.15	38.12	12	16	8
125	36.29	37.11	36.01	32.65	12	−10	−6
126	36.01	32.65	35.77	28.21	12	−10	−4
127	35.77	28.21	35.55	23.83	12	−10	−2
128	35.55	23.83	35.35	19.52	12	−10	0
129	35.35	19.52	35.17	15.31	12	−10	2
130	35.17	15.31	30.6	15.38	12	3	10
131	30.6	15.38	26.04	15.23	12	3	9
132	26.04	15.23	21.5	14.86	12	3	8
133	21.5	14.86	17.02	14.27	12	3	8
134	17.02	14.27	12.6	13.48	12	3	7
135	12.6	13.48	8.26	12.49	12	3	6
136	8.26	12.49	7.06	16.91	12	−5	3
137	7.06	16.91	5.72	21.44	12	−5	2
138	5.72	21.44	4.24	26.04	12	−5	1
139	4.24	26.04	2.58	30.7	12	−5	0
140	2.58	30.7	0.71	35.37	12	−5	−1
141	0.71	35.37	−1.4	40.02	12	−5	−2
142	−1.4	40.02	−3.81	44.61	12	−5	−3
143	−3.81	44.61	−6.58	49.11	12	−5	−3
144	−6.58	49.11	−0.29	48.01	12	6	−2
145	−0.29	48.01	5.74	46.62	12	6	−3
146	5.74	46.62	11.5	44.96	12	6	−4
147	11.5	44.96	16.94	43.06	12	6	−5
148	41.09	39.15	46.79	37.17	12	13	−6
149	46.79	37.17	52.17	34.93	12	13	−9
150	52.17	34.93	57.23	32.44	12	13	−12
151	57.23	32.44	61.96	29.75	12	13	−15
152	61.96	29.75	60.28	25.25	12	27	4

Table A1 (*Continued*).

Element number	Element start		Element end		locking depth	Components (mm/yr)	
	Long	Lat	Long	Lat	(km)	Right Lateral	Opening
153	60.28	25.25	58.76	20.79	12	27	1
154	58.76	20.79	57.39	16.4	12	27	−2
155	57.39	16.4	56.15	12.11	12	27	−5
156	56.15	12.11	52.09	13.12	12	6	26
157	52.09	13.12	47.95	13.94	12	6	23
158	47.95	13.94	43.74	14.59	12	6	20
159	43.74	14.59	39.47	15.05	12	6	17
160	39.47	15.05	35.17	15.31	12	6	14

Element numbers correspond to locations given in Fig. A1. Depth indicates depth to the base of the locked zone. Right lateral slip and opening of an element is positive.

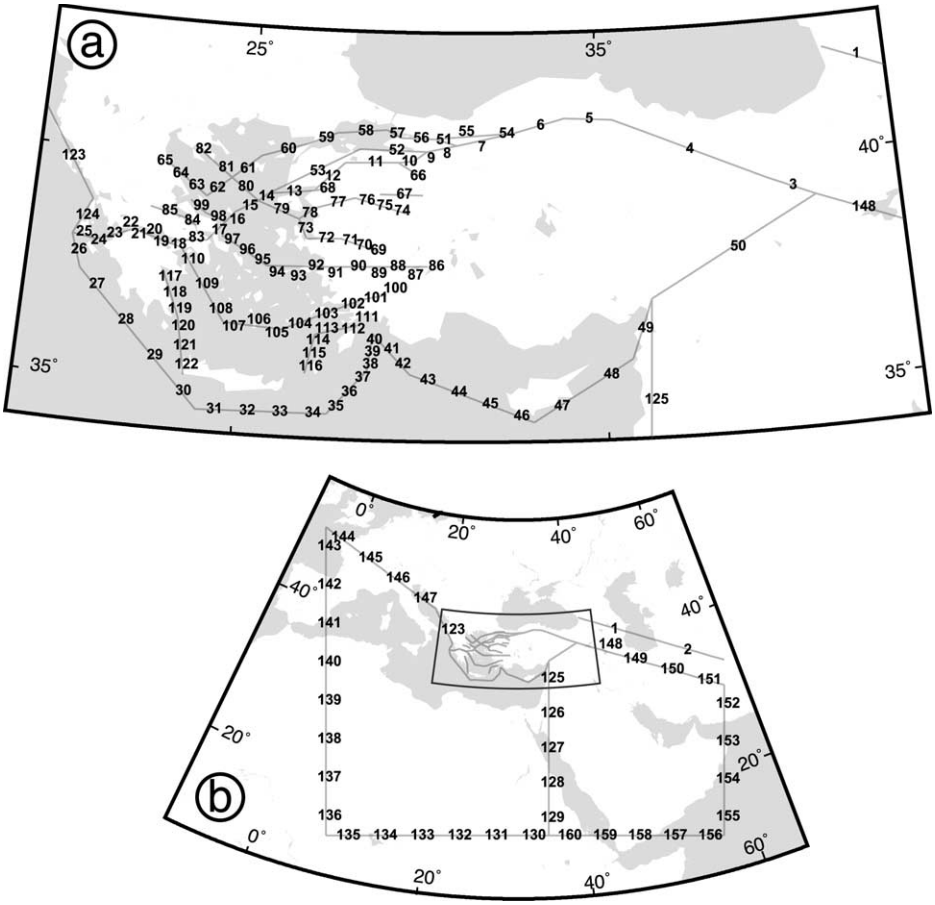

Fig. A1. (a) The elements visible in Fig. 1 in the main text are shown. The numbers identify the corresponding elements in Table A1. (b) Elements of the model over a larger region than that where GPS velocity vectors are modelled in detail. The slip values on these arbitrary boundaries are adjusted to ensure the motions that surround the study region to conform to known plate rates and observed GPS vectors. The numbers identify the corresponding elements in Table A1.

structures evolve by propagation processes consistent with linear elastic fracture mechanics applying at a large scale.

Our approach has implications relevant to the evolution of structures in the Anatolia–Aegean region, which will be the subject of future papers.

Acknowledgements

This work is part of programmes led by the French INSU-CNRS, with support from the French Ministry of Foreign Affairs (MAE) and INSU IT programme Dynamique de la fracturation lithosphérique. We wish to thank J. Muller and M. Abelson for helpful reviews. This is Institut de Physique du Globe de Paris (IPGP) paper No. 1955. INSU paper No. 357.*[VC]*

Appendix

The deformation model is calculated using the dislocation code of Okada [40] in a similar manner to that described by Flerit et al. [38]. Table A1 provides the latitude and longitude of elements used to calculate the vector field shown in Fig. 1 of the manuscript. Fig. A1 shows the location of the elements in map form.

References

[1] J. Angelier, N. Lyberis, X. Le Pichon, E. Barrier, P. Huchon, The tectonic development of the Hellenic arc and the Sea of Crete, a synthesis, Tectonophysics 86 (1982) 159–196.

[2] J.L. Mercier, D. Sorel, P. Vergely, Extensional tectonics regimes in the Aegean basins during the Cenozoic, Basin Res. 2 (1989) 49–71.

[3] G. Seyitoglu, B.C. Scott, C.C. Rundle, Timing of the Cenozoic extensional tectonics in western Turkey, J. Geol. Soc. London 149 (1992) 533–538.

[4] L. Jolivet, J.P. Brun, P. Gautier, S. Lallemant, M. Patriat, 3D-kinematics of extension in the Aegean region from the early Miocene to the present, insights from the ductile crust, Bull. Soc. Géol. Fr. 165 (1994) 195–209.

[5] R. Armijo, B. Meyer, G.C.P. King, A. Rigo, D. Papanastassiou, Quaternary evolution of the Corinth Rift and its implications for the late Cenozoic evolution of the Aegean, Geophys. J. Int. 126 (1996) 11–53.

[6] A.M.C. Sengör, N. Görür, F. Saroglu, Strike-slip faulting and related basin formation in zones of tectonic escape: Turkey as a case study, in: K.T. Biddle, N. Christie-Blick (Eds.), Strike-slip Faulting and Basin Formation, Soc. Econ. Paleontol. Min. Spec. Publ. (1985) 227–267.

[7] A. Hubert-Ferrari, R. Armijo, G.C.P. King, B. Meyer, A. Barka, Morphology, displacement and slip rates along the North Anatolian Fault, Turkey, J. Geophys. Res. 107, B10 (2002) ETG9-1–ETG9-33.

[8] C. Schindler, 1998. Geology of NW Turkey: results of the Marmara polyproject, in: C. Schindler, M. Pfister (Eds.), Active Tectonics of Northwestern Anatolia – The Marmara Poly-Project, A Multidisciplinary Approach by Space-geodesy, Geology, Hydrology, Geothermics and Seismology, Verlag der Fachvereine, Zurich.

[9] R. Armijo, B. Meyer, A. Hubert-Ferrari, A. Barka, Propagation of the North Anatolian Fault into the Northern Aegean: Timing and kinematics, Geology 27 (1999) 267–270.

[10] D.P. McKenzie, Active tectonics of the Alpine-Himalayan belt: The Aegean Sea and surrounding regions, Geophys. J. R. Astron. Soc. 55 (1978) 217–254.

[11] X. Le Pichon, J. Angelier, The Aegean Sea, Phil. Trans. R. Soc. London Ser. A 300 (1981) 357–372.

[12] P.C. England, D. McKenzie, A thin viscous sheet model for continental deformation, J. R. Astron. Soc. 70 (1982) 295–321.

[13] P.C. England, G.A. Houseman, L. Sonder, Length scales for continental deformation on convergent, divergent and strike-slip environments: Analytical and approximate solutions for a thin viscous sheet model, J. Geophys. Res. 90 (1985) 3351–3357.

[14] D. McKenzie, J.A. Jackson, The relationship between strain rates, crustal thickening, paleomagnetism, finite strain and fault movements within a deforming zone, Earth Planet. Sci. Lett. 65 (1983) 182–202.

[15] P. Molnar, Continental tectonics in the aftermath of plate tectonics, Nature 335 (1985) 131–137.

[16] T. Taymaz, J.A. Jackson, D.P. McKenzie, Active tectonics of the north and central Aegean Sea, Geophys. J. Int. 106 (1991) 433–490.

[17] J.A. Jackson, J. Haines, W. Holt, The horizontal velocity field in the deforming Aegean Sea region determined from the moment tensor of earthquakes, J. Geophys. Res. 97 (1992) 17657–17684.

[18] R. Noomen, T.A. Springer, B.A.C. Ambrosius, K. Herzberger, D.C. Kuijper, G.J. Mets, B. Overgaauw, K.F. Wakker, Crustal deformations in the Mediterranean area computed from SLR and GPS observations, J. Geodyn. 21 (1996) 73–96.

[19] R.E. Reilinger, S.C. McClusky, M.B. Oral, R.W. King, M.N. Toksoz, A.A. Barka, I. Kinik, O. Lenk, I. Sanli, Global Positioning System measurements of present-day crustal movements in the Arabia-Africa-Eurasia plate collision zone, J. Geophys. Res. 102 (1997) 9983–9999.

[20] S. McClusky, S. Balassanian, A. Barka, C. Demir, S. Ergintav, I. Georgiev, O. Gurkan, M. Hamburger,

K. Hurst, H. Kahle, K. Kastens, G. Kekelidze, R. King, V. Kotzev, O. Lenk, S. Mahmoud, A. Mishin, M. Nadariya, A. Ouzounis, D. Paradissis, Y. Peter, M. Prilepin, R. Reilinger, I. Sanli, H. Seeger, A. Tealeb, N. Toksöz, G. Veis, Global Positioning System constraints on the plate kinematics and dynamics in the eastern Mediterranean and Caucasus, J. Geophys. Res. 105 (2000) 5695–5719.

[21] B.J. Meade, B.H. Hager, S. McClusky, R. Reilinger, S. Ergintav, O. Lenk, A. Barka, H. Ozener, Estimates of seismic potential in the Marmara Sea region from block models of secular deformation constrained by Global Positioning System measurements, Bull. Seismol. Soc. Am. 92 (2002) 208–215.

[22] J.-P. Avouac, P. Tapponnier, Kinematic model of active deformation in central Asia, Geophys. Res. Lett. 20 (1993) 895–898.

[23] W. Thatcher, GPS constraints on the kinematics of continental deformation, Int. Geol. Rev. 45 (2003) 191–212.

[24] A. Hubert-Ferrari, G.C.P. King, I. Manighetti, R. Armijo, B. Meyer, P. Tapponnier, Long-term elasticity in the continental lithosphere; Modelling the Aden Ridge propagation and the Anatolian extrusion process, Geophys. J. Int. 153 (2003) 111–132.

[25] D. Bowman, G. King, P. Tapponnier, Slip Partitioning by elasto-plastic propagation of oblique slip at depth, Science 300 (2003) 1121–1123.

[26] C.H. Scholz, The Mechanics of Earthquakes and Faulting, Cambridge University Press, Cambridge, 1990, 439 pp.

[27] I. Manighetti, G.C.P. King, C.G. Sammis, The role of fault damage in the evolution of normal faults, Earth Planet. Sci. Lett. (2003) (in press).

[28] P. Lundgren, D. Giardini, R. Russo, A geodynamic framework for eastern Mediterranean kinematics, Geophys. Res. Lett. 25 (1998) 4007–4010.

[29] L.M. Flesh, W.E. Holt, A.J. Haines, B. Shen-Tu, Dynamics of the Pacific-North American plate boundary in the western United States, Science 287 (2000) 834–836.

[30] S. Cianetti, P. Gasperini, C. Giunchi, E. Boschi, Numerical modelling of the Aegean-Anatolian region: geodynamical constraints from observed rheological heterogeneities, Geophys. J. Int. 146 (2001) 760–780.

[31] E. Kendrick, M. Bevis, J.R.F. Smalley, B. Brooks, An integrated crustal velocity field for the central Andes, Geochem. Geophys. Geosyst. 2 (2001) 10.1029/2001GC000191.

[32] A.-S. Provost, J. Chéry, R. Hassani, 3-D mechanical modeling of the GPS velocity field along the north Anatolian fault, Earth Planet. Sci. Lett. 209 (2003) 361–377.

[33] W. Thatcher, Continuum versus microplate models of active continental deformation, J. Geophys. Res. 100 (1995) 3885–3894.

[34] E. Norabuena, L. Leffler-Griffin, A. Mao, T.H. Dixon, S. Stein, I.S. Sacks, L. Ocola, M. Ellis, Space geodetic observations of Nazca-South America convergence across the central Andes, Science 279 (1998) 358–361.

[35] T.H. Dixon, M. Miller, F. Farina, H. Wang, Present-day motion of the Sierra Nevada block and some tectonic implications for the Basin and Range province, North American Cordillera, Tectonics 19 (2000) 1–24.

[36] S. McClusky, S.C. Bjornstad, B.H. Hager, R.W. King, B.J. Meade, M.M. Miller, F.C. Monastero, B.J. Souter, Present day kinematics of the Eastern Cordillera Shear Zone from a geodetically constrained block model, Geophys. Res. Lett. 28 (2001) 3369–3372.

[37] X. Le Pichon, N. Chamot-Rooke, C. Rangin, A.M.C. Sengor, The North Anatolian Fault in the Sea of Marmara, J. Geophys. Res. 108 (2003) ETG1-1–ETG1-20.

[38] F. Flerit, R. Armijo, G.C.P. King, B. Meyer, A. Barka, Slip partitioning in the Sea of Marmara Pull-Apart determined from GPS velocity vectors, Geophys. J. Int. 154 (2003) 1–7.

[39] C. DeMets, R.G. Gordon, D.F. Argus, S. Stein, Effect of recent revisions to the geomagnetic reversal time scale on estimates of current plate motions, Geophys. Res. Lett. 21 (1994) 2191–2194.

[40] Y. Okada, Surface deformation to shear and tensile faults in a half space, Bull. Seismol. Soc. Am. 75 (1985) 1135–1154.